Accepted Manuscript


Influence of low velocity impact on fatigue behaviour of woven hemp fibre reinforced epoxy composites

Davi S. de Vasconcellos, Fabrizio Sarasini, Fabienne Touchard, Laurence Chocinski-Arnault, Monica Pucci, Carlo Santulli, Jacopo Tirillò, Salvatore Iannace, Luigi Sorrentino

PII: S1359-8368(14)00181-4
DOI: http://dx.doi.org/10.1016/j.compositesb.2014.04.025
Reference: JCOMB 3010

To appear in: *Composites: Part B*

Received Date: 13 February 2014
Revised Date: 9 April 2014
Accepted Date: 24 April 2014

Please cite this article as: de Vasconcellos, D.S., Sarasini, F., Touchard, F., Chocinski-Arnault, L., Pucci, M., Santulli, C., Tirillò, J., Iannace, S., Sorrentino, L., Influence of low velocity impact on fatigue behaviour of woven hemp fibre reinforced epoxy composites, *Composites: Part B* (2014), doi: http://dx.doi.org/10.1016/j.compositesb.2014.04.025

# Influence of low velocity impact on fatigue behaviour of woven hemp fibre reinforced epoxy composites

Davi S. de Vasconcellos[a,*], Fabrizio Sarasini[b], Fabienne Touchard[a], Laurence Chocinski-Arnault[a], Monica Pucci[a], Carlo Santulli[b], Jacopo Tirillò[b], Salvatore Iannace[c], Luigi Sorrentino[c]

[a]*Institut Pprime, CNRS-ISAE-ENSMA-Université de Poitiers, Département Physique et Mécanique des Matériaux, ENSMA, 1, Avenue Clément Ader, 86961 Futuroscope Chasseneuil, France*
[b]*Sapienza Università di Roma, Department of Chemical Engineering Materials Environment, via Eudossiana 18, 00184 Rome, Italy*
[c]*Institute for Composite and Biomedical Materials (IMCB)-CNR, P.le E. Fermi 1, 80055 Portici (NA), Italy*

**Abstract**

The purpose of this work is to study the resistance to low velocity impact of woven hemp/epoxy matrix composites and the influence of impact damage on their residual quasi-static tensile and cyclic fatigue strengths. Impact characteristic parameters were evaluated and critically compared to those found in the literature for other similar composites. Damage mechanisms were analysed by using AE monitoring and microscopic observations. An analytical model is used to predict the fatigue lifetime of impacted specimens. Moreover a damage scenario is proposed, reduced to two phases in post-impacted fatigue behaviour, instead of three phases for non impacted specimens.

*Keywords:* A. Fabrics/textiles; B. Impact behaviour; B. Fatigue; C. Acoustic emission

## 1. Introduction

In recent years, as a result of environmental and economical concerns, there has been a growing scientific and economic interest in natural fibres because of their sustainable and eco-friendly production processes and disposal [1, 2], accompanied by good mechanical properties [3]. Bast fibres (hemp, flax and jute) and leaf fibres (sisal) have been considered very promising candidates in terms of specific mechanical properties for semi-structural applications as viable replacement of synthetic reinforcing materials, such as glass and aramid fibres, in polymer based composites [3, 4]. In service conditions, low-velocity impacts and related damage are unavoidable and are often undetectable by human eye inspections. Various research programs have been conducted in order to obtain a better understanding of the behaviour

*Corresponding author: davi.vasconcellos@imcb.cnr.it
*Present address: Institute for Composite and Biomedical Materials (IMCB)-CNR, P.le E. Fermi 1, 80055 Portici (NA), Italy

"The results of this work have been presented at the 4th Conference of Natural Fibre Composites, Rome 17-18 October 2013"

of composite materials under impact [5]. However, there is still a very limited scientific literature on the impact response of natural fibre (woven) composites [6].

In particular for hemp fibres, Scarponi et al. [7] studied the low velocity impact behaviour of a hemp fibre/epoxy composite with 14 layers of 0°/90° oriented fabric. They compared the results from hemp fibre reinforced composites with those obtained in similar conditions on glass fibre fabric/vinylester and jute fibre fabric/vinylester composites, although the latter were prepared with different number of layers and thickness. As a result, they concluded that the hemp/epoxy composite has a good impact behaviour with respect to the mentioned composites. Sabeel Ahmed et al. [8] studied the tolerance to low velocity impacts of a woven jute/polyester composite. They tested composites with 100% jute fabric and hybrid composites, made of jute fabric with the addition of plies of glass fabric. They showed that the composites reinforced with jute have a greater capacity to absorb the impact energy but less tolerance to damage than the hybrid glass/jute composites.

In order to consider synthetic fibre substitutes for industrial applications, it is essential to know the residual mechanical behaviour after impact of natural fibre reinforced structures. Nevertheless, very few data on natural fibre composites are available also on this aspect, in particular on woven natural fibres. Yuanjian et al. [9] studied the effect of low velocity impacts on the strength of glass fibre (0/90)/polyester composites and Sabeel Ahmed et al. [8] studied the post-impact behaviour of hybrid composites based on (jute fabric and glass mat)/ polyester resin. These studies have generally shown that the influence of impact is lower on the Young's modulus than on the tensile strength. Yuanjian et al. explained that low energy impacts only cause damage in the matrix and at the fibre/matrix interface, whereas the composite Young's modulus is manly related to the fibres [9].

Regarding the fatigue behaviour, Yuanjian et al. [9, 10] studied the post-impact fatigue behaviour of hemp(mat)/polyester and glass/polyester composites. They showed that, as expected, the impact causes a decrease in the fatigue lifetime of the composite but they stated that when the S-N curves are normalized with respect to the corresponding residual strength, there is a single curve for the impacted and non-impacted specimens. This result has also been detected in post-impact compression fatigue tests on carbon/epoxy composites [11]. This finding shows that the S-N curve after impact can be deduced from the residual strength of the damaged composite and the S-N curve of the non-impacted composite [12].

In the scientific literature, data on the post-impact fatigue behaviour of composites reinforced with woven natural fibres are not yet reported and this study aims to fulfil this gap by providing experimental data and

modelling tools to enable a good estimation of them. The purpose of this work is to study the resistance to low velocity impact of woven hemp/epoxy matrix composites and the influence of impact damage on their residual quasi-static tensile and cyclic fatigue strengths. Drop weight impact tests were performed on woven hemp/epoxy composite specimens to analyse their impact behaviour and damage modes. Impacted samples were tested in quasi-static and cyclic fatigue tensile loading and compared with results from non-impacted ones. Finally, an analytical model was used to predict S-N curves after impact.

## 2. Materials and methods

### 2.1. Fabrication of composite materials

The studied composite materials have already been used in previous studies [13 - 16] and are characterized by a lay-up of 7 plies of a plain woven hemp fabric impregnated with epoxy resin. The hemp fabric (produced by *Lin et L'Autre* – France) has non-treated surface, a weight of 267 ± 1 g/m$^2$ and a thread count of 2362 x 1575 (warp and weft per metre) with three hemp yarns in each warp and weft strand. Hemp fibres in yarns have an average diameter of 13 ± 5 µm and are produced with a twist level of 324 tpm (yarn surface twist angle of 11°) and a linear density of 83 tex. Besides the irregular cross-section, the hemp yarns have an apparent diameter of 300 ± 60 µm [13]. The epoxy resin is an EPOLAM 2020 from *Axson Technologies* (France) with density of 1.10 g/cm$^3$ after curing (according to the manufacturer's datasheet). The composite plates were manufactured at *Valagro* (France), by the vacuum infusion technique (vacuum of 30 mbar, absolute pressure). The hemp fabric was pre-dried at 40 °C for 24h before use. The laminates were cured by using the following cycle: 24 h at ambient temperature, 3 h at 40 °C, 2h at 60 °C, 2h at 80 °C and 4h at 100 °C. The resulting composite plates are characterised by a density of 1.2 ± 0.1 g/cm$^3$, a fibre volume fraction of 0.31 ± 0.04, a maximum void content of around 6% by volume and a thickness of 4.5 ± 0.2 mm. The composite plates have the warp direction of each ply oriented at 0° from the tensile axis (X axis).

### 2.2. Mechanical characterizations

#### 2.2.1. Low-velocity impact set-up

Impact tests were performed at room temperature by using a falling dart impact testing machine, model Fractovis Plus from CEAST (Pianezza - TO, Italy), with a 22 kN load cell, an hemispherical impact head (diameter equal to 12.7 mm) and a circular sample holder with 40 mm inner diameter. The machine is also equipped with a mechanical anti-rebound brake to prevent multiple impacts on samples. Specimens

were impacted at 2.5 J, 5 J and 10 J by keeping constant the indenter mass (6.929 kg), which resulted in impact velocities of 0.85 m/s, 1.20 m/s and 1.70 m/s, respectively. Impact tests were performed on six square specimens of 50 mm x 50 mm x 4.5 mm (length x width x thickness) for impact test characterization, and nine rectangular specimens of 150 mm x 50 mm x 4.5 mm, to carry out post-impact quasi-static tensile tests (three specimens of each type for each impact energy level). Then other nine rectangular specimens of 150 mm x 50 mm x 4.5 mm were impacted at 5 J to perform post-impact fatigue tests.

#### 2.2.2. Quasi-static tensile and fatigue tests

Samples of 150 mm x 30 mm x 4.5 mm were cut from rectangular impacted specimens at each energy level to perform tensile tests at constant cross-head speed of 0.5 mm/min by means of a universal testing machine (*Zwick/Roell, model Z010*). Specimens impacted at 5 J were tested in tension-tension fatigue with a MTS 858 Mini Bionix dynamic testing machine, by selecting a stress ratio ($R$) equal to 0.01, a frequency ($f$) equal to 1 Hz and three different maximum stresses ($\sigma_{max}$) calculated as 80%, 60% and 40% of the ultimate tensile stress (UTS) from 5J impacted samples ($\sigma_{5J}$).

### 2.3. Damage characterization

Damage development during fatigue tests was monitored by acoustic emission (AE), using an AMSY-5 AE system from *Vallen Systeme GmbH* (Icking, Germany). To allow linear localization of signals, two broad-band PZT AE sensors (100-1500 kHz, *Fujicera* 1045S, 20 mm of diameter) were placed at both ends of specimens using silicon grease for coupling with the laminate, at a distance of 50 mm from each other. The measured amplitude of AE events was corrected by the corresponding attenuation curve, as proposed by Mechraoui et al. [17]. Acquisition parameters were taken from previous works on the same composite [13, 15] , where experimental tests were performed with single hemp yarns, neat epoxy resin and composite specimens. Statistical analysis of AE amplitude signals was performed and correlated with observations at the microscale. Three types of damage were identified in the studied composite structure each one characterized by a peculiar AE amplitude signal range as a discriminating signature. Based on the full width at half maximum criteria of the normal distribution of AE amplitudes, the three amplitude ranges have been identified and related to each damage mode: 35–53 dB for epoxy resin cracks, 58–63 dB for interface damage mechanisms, and 66–100 dB for hemp fibre damage. AE signals with amplitude in the intervals between 53–58 dB and 63–66 dB have an uncertainty to be classified in a single damage mode, so were not considered for damage classification.

Internal damage of impacted specimens was then studied by optical microscopy of cross-sections. The two optical digital microscope systems used are a *Leica Microsystems* device, which allows up to six times magnification and a *Reichert-Jung* system, which enables up to 1000 times magnification.

### 2.4. Data analysis

In literature, in order to analyse fatigue S-N curve results for composite materials, power law based equation regressions have been widely used [18 - 23]. In this work, an empirical model developed by Epaarachchi et al. [18] was used to fit fatigue S-N curve results. Based on the model of D'Amore et al. [24, 25], Epaarachchi et al. use a deterministic equation for the rate of degradation of the composite strength due to fatigue:

$$\frac{d\sigma}{dN} = -C_1 N^{-m_1} \tag{1}$$

where $\sigma$ is the residual strength after $N$ cycles, $C_1$ and $m_1$ are composite related parameters and $N$ is the number of fatigue cycles.

From Eq. (1) and the hypothesis that the final failure takes place when material residual strength after N cycles is equal to the maximum stress during fatigue cycling ($\sigma_{max}$) [24], Epaarachchi et al. proposed an equation to calculate the critical number of cycles to failure ($N_f$):

$$N_f = \left[1 + \left(\frac{\sigma_0}{\sigma_{\max}} - 1\right)\frac{f^{\beta}}{\alpha\,(1-R)^{\lambda-R}}\left(\frac{\sigma_0}{\sigma_{\max}}\right)^{\lambda-1-R}\right]^{\frac{1}{\beta}} \tag{2}$$

where $\sigma_0$ is the static tensile strength of the material before tests, $R$ is the stress ratio, $f$ is the frequency, $\lambda$ is a parameter with a fixed value equal to 1.6 [18], and $\alpha$ and $\beta$ are the only two material parameters to be experimentally evaluated. To identify these two parameters, Eq. (2) can be rearranged in the form:

$$\alpha\left(N_{f^{\beta}} - 1\right) = \left(\frac{\sigma_0}{\sigma_{\max}} - 1\right)\frac{f^{\beta}}{(1-R)^{1,6-R}}\left(\frac{\sigma_0}{\sigma_{\max}}\right)^{0,6-R} \tag{3}$$

where all experimental results should converge to a single straight line passing through the origin when the expression on the right side is plotted against ($N_f^{\beta}$ - *1*). Once determined a $\beta$ value for which the experimental results best fit a straight line passing through the origin, then the line slope value will define $\alpha$.

## 3. Results and Discussion

### 3.1. Low-velocity impact tests

### 3.1.1. Characteristic parameters

Fig. 1a presents the contact force-deflection curve of specimens impacted at 2.5 J, 5 J and 10 J. In this curve, contact force is the load undergone by the specimen and deflection is the indentation of the falling dart through the specimen's surface. These plots show a closed loop, which is peculiar to specimens having rebound. As schematized in Fig. 1b, the area under the curve is the deformation energy that is initially transferred from the dart to the specimen and then returned from the specimen to the (rebounding) dart (i.e. recovered energy). From this curve, also other characteristic parameters were obtained, like peak load and linear stiffness, to characterize the laminate resistance to impacts and to allow comparisons between different materials.

The peak load indicates the maximum load that the composite can bear before undergoing to major damages [26]. Fig. 2a presents a comparison of the peak load values for the tested hemp/epoxy composites and selected data available in literature for glass/epoxy [27] and Kevlar/epoxy [28] fabric reinforced composites. Even though these data depend on the amount of fibres in the composite and also on the thickness of samples, they show that hemp fibres are comparable to synthetic ones in terms of impact resistance in reinforced composites.

In the graph of Fig. 2b, the ratio between absorbed and impact energy is plotted for different impact energies and compared to data (green points) from a similar hemp/epoxy composite [7] to observe the trend for higher impact energy. These results show that this ratio increases with the impact energy level, which indicates growing impact damage for increasing impact energy.

### 3.1.2. Damage analysis

Surface damage modes were analysed and are presented in Fig. 3 for specimens impacted at 2.5 J, 5 J and 10 J. Pictures on the left show the impacted sides (front face), where the damage appears as a circular indentation caused by the falling hemispherical head. The depth of this indentation increased with increasing impact energy and there were no visible crack or perforation on the front face for the applied impact energies. The damage on the opposite sample side (back face) starts with ± 45° oriented cracks with respect to warp yarns in the specimen impacted at 2.5 J and proceed in the radial direction from the centre of the specimen, in samples impacted at 5 J and 10 J. For these higher energies, the crack tends to propagate along the direction of fabric yarns, as clearly visible in Fig. 3. This pattern of matrix cracking is characteristic of woven composites [7, 8, 29]. Finally, as expected, pictures show that the damage of both faces increases with the impact energy.

The damage visible on the back face is an indicator of the impact resistance of a composite material and it is interesting to compare its size with that of other types of composites even if there is no uniform standard for comparison. In this study, the damage size is considered as the area of the ellipse encompassing the damage. In Fig. 4, the back face damage size is measured on the studied hemp/epoxy composites and plotted versus the impact energy showing that the damaged area at the back face increases significantly with the impact energy. This figure also shows the size of the damaged area for some synthetic fibre and epoxy matrix composites (two values from glass fibres reinforced composites [27, 30] and one from woven Kevlar reinforced composites [28]), in which the impact test conditions are comparable with those used in this work. Results from the literature were obtained by determining the number of pixels in the damaged zone in sample pictures, while in this work the ellipse surface is considered, which leads to an overestimated value in comparison with the former method. However, Fig. 4 clearly shows that the damaged area of the studied hemp/epoxy composites is comparable to that obtained from the considered synthetic fibre composites.

Impacted specimens were cut, along the warp yarn direction, in the centre of the damaged zone through specimen thickness, with a diamond wire cutting process, and then polished. Optical microscope observations revealed a brighter area in the matrix with a conical shape (Fig. 5), which corresponds to the internal damage that grows toward the back face, a characteristic phenomenon present in impacted composite materials [31 - 34]. It has also been observed that the damaged area increases with the impact energy. For impact energy of 2.5 J, the conical zone reaches the $4^{th}$ and $5^{th}$ plies far from the impacted face (Fig. 5). At impact energy of 5 J, the conical region reaches the $1^{st}$ and $2^{nd}$ plies from the front face. Finally at impact energy of 10 J, damage expands in the laminate and a residual deflection of the sample is visible.

Samples impacted at 5 J were then cut at 90° and 45° from the warp yarn direction to observe the damage along the directions outlined in the sketches (Fig. 6). In these photos, semi-conical brighter areas representing damage are present in the cross-sections. These observations are in very good agreement with the theoretical shape of the back face damaged area in the XY plane as represented in Fig. 7. A significant difference is observed in the size of the cone base for the 45° cross-section, which is substantially lower than those in 0° and 90° cross-sections. This indicates that the damage spreads easily in yarns directions, even if it is initially oriented at 45°.

At higher magnification (Fig. 8), it was possible to distinguish two types of internal damage: interface (Fig. 8a and Fig. 8b) and matrix (Fig. 8c) cracks, located in the conical zone previously observed. No yarn or fibre breakage was found in any observed specimen. Indeed, according to the literature [35, 36], for relatively low impact energies, the damage starts with the composite matrix cracking and debonding at the fibre/matrix interface while fibre damage occurs only for higher energy levels. The damage at the yarn/matrix interface ("type 1") tends to bypass the yarns of each strand and it has been found around both weft (Fig. 8a) and warp (Fig. 8b) yarns. For the three levels of impact energy used, this type of crack was found through the whole thickness of the specimen just below the impacted area. The Fig. 8c shows matrix cracks ("type 2"). This type of crack is generally connected to interface cracks or initial manufacturing defects (pores). For specimens impacted at 2.5 J, the matrix cracks are present from the $4^{th}$ to $7^{th}$ ply from the front face. For specimens impacted at 5 J, these cracks are present from the $2^{nd}$/$3^{rd}$ to the $7^{th}$ ply. Finally, for specimens impacted at 10 J, these cracks were found throughout the thickness of the composite. The qualitative evolution in the distribution of both types of damage for the three impact energies is shown in the diagrams of Fig. 9, coupled with photos showing conical damage areas from sample cross sections. These pictures show a clear similarity between the qualitative evolution of matrix cracks ("type 2") and the bright areas in all samples.

It should be noted that no delamination was observed, whatever the impact energy level was used. This is characteristic of woven reinforcements, which are known to be highly resistant to delamination.

**3.2. Static tensile tests**

Impacted specimens were tested in quasi-static tensile tests to analyse the influence of impact damage on residual tensile strength and stiffness. Systematically for each level of impact energy, the final failure of specimens tested in tension occurred in the area previously damaged by impact, as shown in Fig. 10. It has been observed that the final failure of impacted specimens is asymmetrical between the front and back faces. On the back face, the tensile failure tends to follow the 45° defect at the centre of the damage created by the impact, while on the front face the failure is always oriented perpendicularly to the tensile axis. This asymmetry of the specimen tensile failure is due to the asymmetry of the impact damage.

Fig. 11a compares the ultimate tensile stress (UTS) of as-manufactured and impacted specimens at different impact energies. These tests indicate that tensile strength of composites is reduced to about 85% after an impact at 2.5 J, to 70% after an impact at 5 J, and to about 60% after an impact at 10 J. One can also observe the increase in standard deviation of UTS for impacted specimens compared to non-

impacted ones. This higher standard deviation is probably due to the combined effect of data dispersion from the material tensile strength and data dispersion from impact tests, partly related to the data dispersion of mechanical properties of natural plant fibres. On the other hand, the elastic stiffness of impacted specimens does not present significant change as it remains into the data dispersion of non-impacted ones, as represented by dashed lines in Fig. 11b. This can be related to the absence of fibre damaging during impact tests at the used impact energies, as previously confirmed by the optical microscope analysis.

### 3.3. Fatigue tests

Based on results of impact tests and post-impact tensile tests, the 5 J impact energy level was selected for post-impact fatigue testing, since it produced significant but not close-to-failure damage, suggesting that after impact at 5 J, the composite may still continue to be used in service conditions. Final fatigue failure mode of impacted specimens has been observed to be similar to the quasi-static one (Fig. 10), since the laminate failure occurs in the impacted region with an asymmetry between the front and the back faces.

#### 3.3.1. S-N curves

In Fig. 12, the maximum fatigue stress ($\sigma_{max}$) normalised by the mean UTS of non-impacted specimens ($\sigma_0$) is plotted (red circles) against the number of cycles to failure for each tested specimen. Also, results from previous fatigue tests [16] on non-impacted specimens of the same material are added (blue squares). For both impacted and non-impacted specimens results, the arrows represent specimens that did not fail after $10^6$ fatigue cycles. The power-law model of Epaarachchi et al. [18] was used to fit the experimental points (solid lines). To adapt this model to the results of impacted specimens, the equation of the number of cycles to failure ($N_f$), Eq.(2), was modified to:

$$N_f = \left[1 + \left(\frac{\sigma_{5J} \pm \Delta}{\sigma_{\max}} - 1\right) \frac{f^{\beta}}{\alpha (1-R)^{1,6-R}} \left(\frac{\sigma_{5J} \pm \Delta}{\sigma_{\max}}\right)^{0,6-R}\right]^{\frac{1}{\beta}} \quad (4)$$

where $\sigma_{5J}$ is the residual tensile strength of 5 J impacted specimens and the material parameters $\alpha$ and $\beta$ used were the same as those experimentally determined in previous work on non-impacted specimens [16]. The dashed lines represent the standard deviation for the power-law model, based on the standard deviation ($\Delta$) of the UTS. Fig. 12 shows that fatigue strength, as expected, decreases with the increase in fatigue stress for both impacted and non-impacted composites. For a given fatigue stress, the number of cycles to failure is reduced for impacted specimens compared to non-impacted ones. Also, it is worth to

note the more larger dispersion of fatigue data resulting for impacted specimens compared to non-impacted ones, as also experienced in tensile tests.

The good fit of the S-N curve model for impacted specimens using material parameters from non-impacted ones means that, for the studied composite and for low energy impacts, the influence of impact on the fatigue behaviour can be determined from the influence of impact load on the laminate tensile strength. It is thus possible to predict the fatigue life of impacted specimens just knowing the fatigue life of non-impacted specimens and the residual UTS for the given impact energy. For example, in Fig. 13 are shown the S-N curves for non-impacted specimens and predicted S-N curves with Eq.(4), using the residual tensile strengths of specimens impacted at 2.5 J, 5 J and 10 J.

### 3.3.2. Acoustic Emission (AE) monitoring

AE events, which are related to occurrence of damage, were recorded during fatigue tests and are presented in Fig. 14 (left side). The vertical axis represents the specimen's gauge length between AE sensors and the horizontal axis represents the normalized fatigue cycles. These figures are related to impacted specimens tested in fatigue with stress levels of 40%, 60% and 80% of the UTS from impacted specimens ($\sigma_{5J}$). The curves on the right side represent the number of acoustic events per family of damage along the specimen's gauge length. For all applied fatigue stress levels, the AE events are distributed all along fatigue lifetime, but they are concentrated in the impacted zone where also ultimate failure occurred, as represented by a cross in the vertical axis. The distributions of damage mechanisms are separated by family and show that mainly fibre related events are concentrated in this area. These three figures show also a growing amount of AE events for higher fatigue stress level.

In Fig. 15a are represented the curves of the cumulative number of acoustic events plotted against the position for the impacted specimens for three stress levels. Comparing the curves in this figure with those obtained from non-impacted specimens (Fig. 15b), it is evident that the acoustic events are distributed more uniformly over the entire length of the specimen and along fatigue lifetime [16] in the case of non-impacted specimens.

Another significant difference between AE events on impacted and non-impacted specimens during fatigue tests emerges from Fig. 16, where the cumulative numbers of AE events for impacted and non-impacted specimens are plotted against normalized fatigue cycles, for fatigue stress levels of 40%, 60% and 80% of the respective UTS. This evolution of acoustic events indicates the development of material's damage during fatigue testing. In particular, for non-impacted specimens, curves at the three stress levels

show the same global trend: a sudden and significant increase during initial cycles (phase I), then a slower increase at a constant rate during most fatigue lifetime (phase II) and, finally, a quick and high increase just before failure (phase III). On the other hand, the curves for the impacted specimens show only two marked phases: a small and constant raise during most fatigue lifetime (phase II') and a fast increase at final cycles (phase III').

In the previous work [16], damage mechanisms of non-impacted specimens for each one of the three observed phases has been proposed, based on damage observations and on the mechanisms proposed by Reifsnider et al. [37] and Schulte et al [38] applied to other types of composite materials. According to the proposed scenario for non-impacted composites, results for impacted specimens show that phase I, which is characterized by the initial damage of the yarn/resin interface and the creation of transverse microcracks in the matrix, is almost nonexistent. Moreover, it was shown in Fig. 8 that these damages are already generated by impacts. Thus, one can conclude that the phase I has been replaced by the mechanical impact, and that fatigue damage of the impacted hemp/epoxy composite consists of two phases: a) Phase II', corresponding to the coalescence and growth of matrix cracks (type 2) and interfacial cracks (type 1), originally created by impact and b) Phase III', characterized by the final development of interface damage, matrix cracks and fibre rupture leading to yarn rupture and final failure of the specimen.

## 4. Conclusions

Impact tests have been performed on woven hemp/epoxy composites. Impact related parameters such as peak load, elastic energy and absorbed energy were studied and compared to those reported in the literature for other composites. Results show that the studied eco-composite has an impact behaviour which is comparable to the one of synthetic composites.

The influence of impact damage on the residual tensile strength and stiffness was also studied. A decrease of the residual tensile strength has been measured, while the elastic modulus remains unchanged. Fatigue tests on 5 J impacted specimens have been performed and a deep analysis of the damage mechanisms and evolution has been realised by using AE monitoring and microscopic observations. It was shown that impacts induce the formation of damages at the fibre/interface and microcracks in the matrix, thus anticipating the Phase II and Phase III of damage evolution in fatigue testing of non-impacted specimens. An analytical model was used to predict the residual fatigue life of the studied composite for any low-energy impact level starting from a small set of data from fatigue characterization of non impacted

specimen and impact tests at low energy level. These results enable a better understanding of the influence of low velocity impact on the fatigue resistance of woven hemp/epoxy composites.

## 5. Acknowledgements

The authors thank Région Poitou-Charentes (France) and Ecole Doctorale SI-MMEA for their financial support.

## References

1 Wambua P, Ivens J, Verpoest I. Natural fibres: can they replace glass in fibre reinforced plastics?. Compos Sci Technol 2003;63;1259–1264.
2 Corbiere-Nicollier T, Gfeller Laban B, Lundquist L, Leterrier Y, Månson J-A, Jolliet O. Life cycle assessment of biofibres replacing glass fibres as reinforcement in plastics. Resour Conserv Recycl 2001;33;267–287.
3 Faruk O, Bledzki AK, Fink H-P, Sain M. Biocomposites reinforced with natural fibres: 2000–2010. Prog Polym Sci 2012;37;1552–1596.
4 Joshi S, Drzal L, Mohanty A, Arora S. Are natural fibre composites environmentally superior to glass fibre reinforced composites?. Compos Part A Appl Sci Manuf 2004;35;371–376.
5 Cantwell WJ, Morton J. The impact resistance of composite materials — a review. Composites 1991;22;347–362.
6 De Rosa IM, Dhakal HN, Santulli C, Sarasini F, Zhang ZY. Post-impact static and cyclic flexural characterisation of hemp fibre reinforced laminates. Compos Part B Eng 2012;43;1382–1396.
7 Scarponi C, Pizzinelli CS, Sanchez-Saez S, Barbero E. Impact load behaviour of Resin Transfer Moulding (RTM) hemp fibre composite laminates. J Biobased Mater Bioenergy 2009;3;298–310.
8 Sabeel Ahmed KS, Vijayarangan S, Kumar A. Low Velocity Impact Damage Characterization of Woven Jute Glass Fabric Reinforced Isothalic Polyester Hybrid Composites. J Reinf Plast Compos 2007;26;959–976.
9 Yuanjian T, Isaac DH. Combined impact and fatigue of glass fibre reinforced composites. Compos Part B Eng 2008;39;505–512.
10 Yuanjian T, Isaac DH. Impact and fatigue behaviour of hemp fibre composites. Compos Sci Technol 2007;67;3300–3307.
11 Komus A. PhD thesis: fatigue behaviour of a barely visible impact damaged carbon fibre reinforced epoxy laminate. University of Manitoba: Manitoba, Canada; 2010.
12 Beheshty MH, Harris B, Adam T. An empirical fatigue-life model for high-performance fibre composites with and without impact damage. Compos Part A Appl Sci Manuf 1999;30;971–987.
13 Bonnafous C. PhD thesis: analyse multi échelle des mécanismes d'endommagement de composites chanvre/époxy à renforts tissés. Caractérisation de l'interface fibre/matrice. Ecole Nationale Supérieure de Mécanique et d'Aérotechnique: Futuroscope Chasseneuil, France; 2010.
14 Guillebaud-Bonnafous C, Vasconcellos D, Touchard F, Chocinski-Arnault L. Experimental and numerical investigation of the interface between epoxy matrix and hemp yarn. Compos Part A Appl Sci Manuf 2012;43;2046–2058.
15 Bonnafous C, Touchard F, Chocinski-Arnault L. Multi scale analysis by acoustic emission of damage mechanisms in natural fibre woven fabrics/epoxy composites. In: Proceedings of ICEM-14 Conference. Poitiers, July, 2010.
16 de Vasconcellos DS, Touchard F, Chocinski-Arnault L. Tension–tension fatigue behaviour of woven hemp fibre reinforced epoxy composite: A multi-instrumented damage analysis. Int J Fatigue 2014;59;159-169.
17 Mechraoui S-E, Laksimi A, Benmedakhene S. Reliability of damage mechanism localisation by acoustic emission on glass/epoxy composite material plate. Compos Struct 2012;94;1483–1494.
18 Epaarachchi JA, Clausen PD. An empirical model for fatigue behavior prediction of glass fibre-reinforced plastic composites for various stress ratios and test frequencies. Compos Part A Appl Sci Manuf 2003;34;313–326.
19 Mandell J, Reed R, Samborsky D, Pan Q. Fatigue performance of wind turbine blade composite materials. Wind Energy 1993;14;191–198.
20 Mandell J, Reed R, Samborsky D. Fatigue of fibreglass wind turbine blade materials. Bozeman: Sandia Contract 40-8875, 1992.

21 Samborsky DD, Wilson TJ, Mandell JF. Comparison of Tensile Fatigue Resistance and Constant Life Diagrams for Several Potential Wind Turbine Blade Laminates. J Sol Energy Eng 2009;131;0110061-01100610.

22 D. Samborsky. PhD thesis: Fatigue of E-glass fibre reinforced composite materials and substructures. Montana State University: Bozeman, USA; 1999.

23 Shah DU, Schubel PJ, Clifford MJ, Licence P. Fatigue life evaluation of aligned plant fibre composites through S–N curves and constant-life diagrams. Compos Sci Technol 2013;74;139–149.

24 D'Amore A, Caprino G, Stupak P, Zhou J, Nicolais L. Effect of Stress Ratio on the Flexural Fatigue Behaviour of Continuous Strand Mat Reinforced Plastics. Sci Eng Compos Mater 1996;5;1–8.

25 Caprino G, D'Amore A. Flexural fatigue behaviour of random thermoplastic composites. Compos Sci Technol 1998;58;957–965.

26 Padaki NV, Alagirusamy R, Deopura BL, Sugun BS, Fangueiro R. Low velocity impact behaviour of textile reinforced composites. Indial J Fibre Text Res 2008;33;189–202.

27 Kang K-W, Kim J-K. Effect of shape memory alloy on impact damage behavior and residual properties of glass/epoxy laminates under low temperature. Compos Struct 2009;88;455–460.

28 Reis PNB, Ferreira JAM, Santos P, Richardson MOW, Santos JB. Impact response of Kevlar composites with filled epoxy matrix. Compos Struct 2012;94;3520–3528.

29 Dhakal HN, Zhang ZY, Richardson MOW, Errajhi OAZ. The low velocity impact response of non-woven hemp fibre reinforced unsaturated polyester composites. Compos Struct 2007;81;559–567.

30 Karakuzu R, Erbil E, Aktas M. Impact characterization of glass/epoxy composite plates: An experimental and numerical study. Compos Part B Eng 2010;41;388–395.

31 Hosur MV, Karim MR, Jeelani S. Experimental investigations on the response of stitched/unstitched woven S2-glass/SC15 epoxy composites under single and repeated low velocity impact loading. Compos Struct 2003;61;89–102.

32 Shyr T-W, Pan Y-H. Impact resistance and damage characteristics of composite laminates. Compos Struct 2003;62;193–203.

33 Petit S, Bouvet C, Bergerot A, Barrau J-J. Impact and compression after impact experimental study of a composite laminate with a cork thermal shield. Compos Sci Technol 2007;67;3286–3299.

34 Tan KT, Watanabe N, Iwahori Y. X-ray radiography and micro-computed tomography examination of damage characteristics in stitched composites subjected to impact loading. Compos Part B Eng 2011;42;874–884.

35 Santulli C, Cantwell WJ. Impact damage characterization on jute reinforced composites. J Mater Sci Lett 2001;20;477–479.

36 Caprino G, Lopresto V, Langella A, Durante M. Irreversibly absorbed energy and damage in GFRP laminates impacted at low velocity. Compos Struct 2011;93;2853–2860.

37 Reifsnider KL, Schulte K, Duke JC. Long-term fatigue behavior of composite materials. In: O'Brien TK, editor. Long-term Behavior of Composites, ASTM STP 813. Philadelphia: American Society for Testing and Materials, 1983. p.136–159.

38 Schulte K, Baron C, Neubert N, Bader MG, Boniface L, Wevers M, Verpoest I, de Charentenay FX. Damage development in carbon fibre epoxy laminates: cyclic loading. In: Proceedings of the MRS-Symposium "Advanced Materials for Transport". Strasbourg, November, 1985.

Figure Captions

Fig. 1 – (a) Impact load-displacement curves for hemp/epoxy composite specimens impacted at 2.5 J, 5 J and 10 J. (b) Schematic representation of impact characteristic parameters.

Fig. 2 – Comparison of results from impact tests of the present work with data from literature reported on woven composites: (a) peak load; (b) ratio between absorbed and impact energy as a function of impact energy.

Fig. 3 – Front and back faces of hemp/epoxy specimens impacted at 2.5 J, 5 J and 10 J.

Fig. 4 – Damaged area on the back face of hemp/epoxy composites impacted at 2.5 J, 5 J and 10 J and comparison with glass/epoxy and Kevlar/epoxy composites from literature data.

Fig. 5 - Microscopic observation of the cross section of hemp/epoxy specimens impacted at 2.5 J, 5 J and 10 J.

Fig. 6 – Comparison of internal damage in the direction of cutting (0°, 90° and 45°) for the hemp/epoxy composite impacted at 5 J.

Fig. 7 – Theoretical shape of damaged area on back face in the XY plane, for the hemp/epoxy composite impacted at 5 J.

Fig. 8 - Internal damage of a 5 J impacted hemp/epoxy composite in different thickness positions.

Fig. 9 - Qualitative distribution of the two types of damage in cross-sections at 0° of specimens of hemp/epoxy composite for each level of impact energy.

Fig. 10 – Optical micrographs of the front and back faces after the final failure of hemp/epoxy composite specimens tested in tension after being impacted at different impact energy levels.

Fig. 11 – Comparison of quasi-static properties of non-impacted and impacted woven hemp/epoxy composites: (a) Ultimate tensile stress and (b) Young's modulus.

Fig. 12 - S-N fatigue curves for 5 J impacted and non-impacted specimens of woven hemp/epoxy composite.

Fig. 13 – Prediction of fatigue lifetime for hemp/epoxy composites impacted at 2.5 J, 5 J and 10 J.

Fig. 14 – Distribution of acoustic events during fatigue tests on hemp/epoxy composite specimens impacted at 5 J (left) and number of acoustic events, per damage mode, along the specimen length (right).

Fig. 15 – Cumulative number of acoustic events along the specimen's gauge length for (a) impacted at 5 J and (b) non-impacted hemp/epoxy composites for the three stress levels studied.

Fig. 16 – Cumulative number of acoustic events versus the normalized number of fatigue cycles for (a) impacted specimens and (b) non-impacted specimens for the three levels of fatigue loading.

(a)

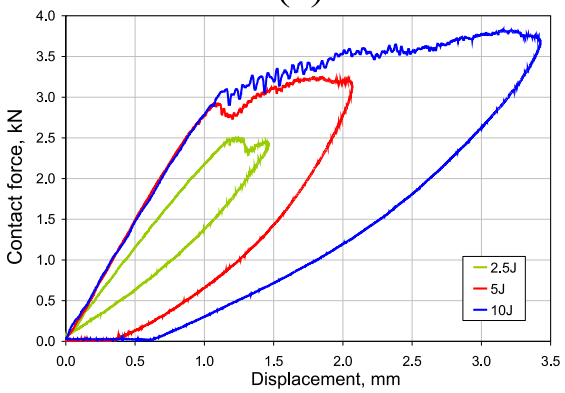


(b)

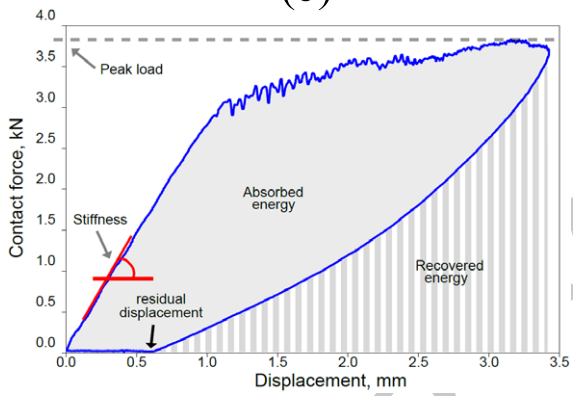


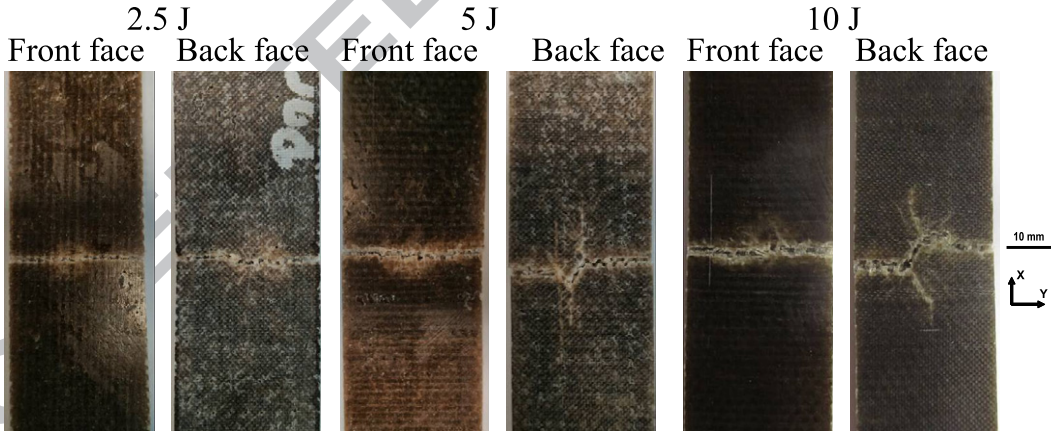

(a)

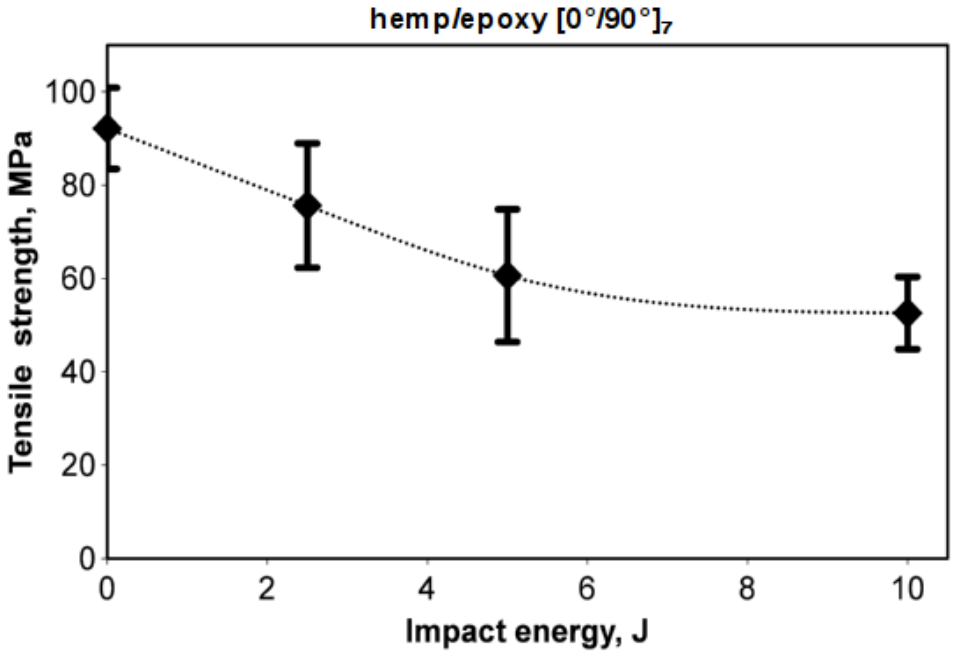
hemp/epoxy [0°/90°]7
Tensile strength, MPa
100
80
60
40
20
0
0
2
4
6
8
10
Impact energy, J

(b)

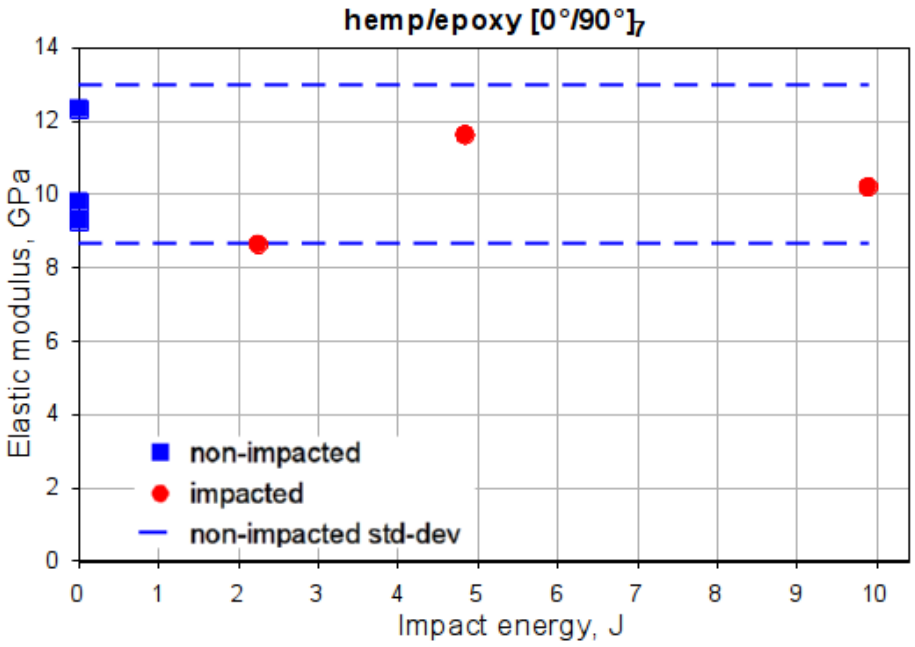
hemp/epoxy [0°/90°]7
Elastic modulus, GPa
14
12
10
8
6
4
2
0
0
1
2
3
4
5
6
7
8
9
10
Impact energy, J
non-impacted
impacted
non-impacted std-dev

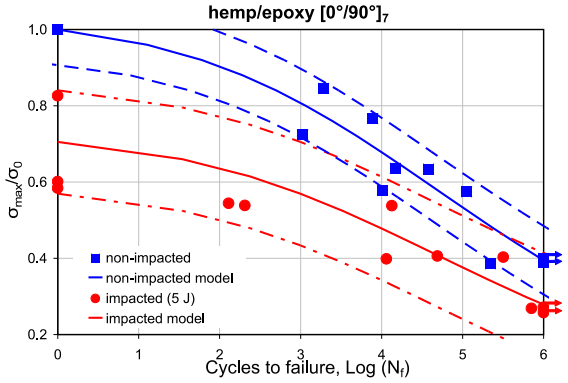


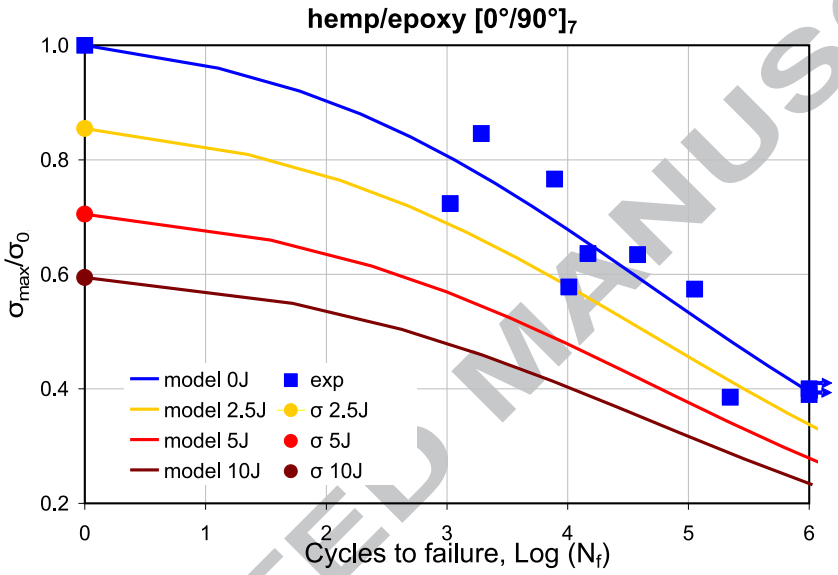

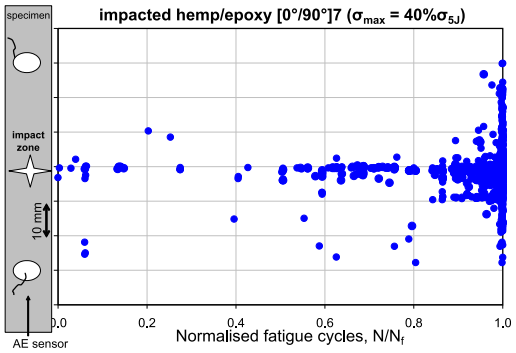


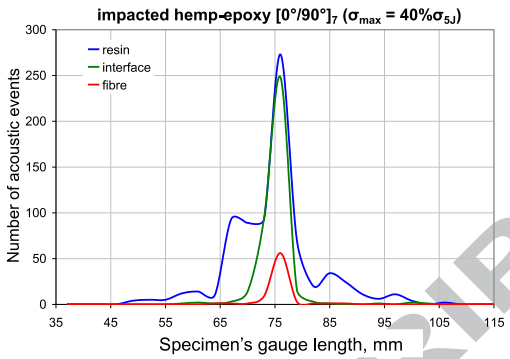


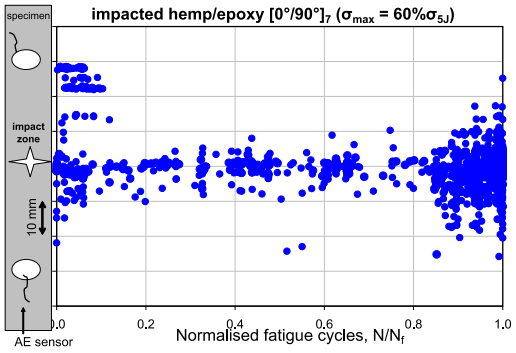


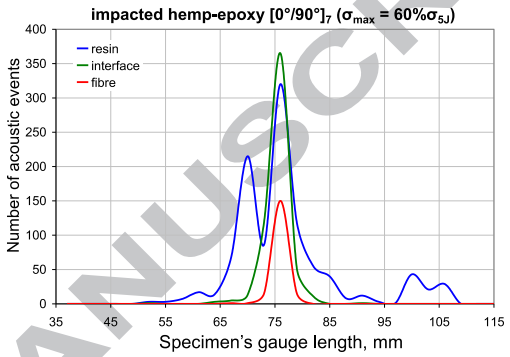


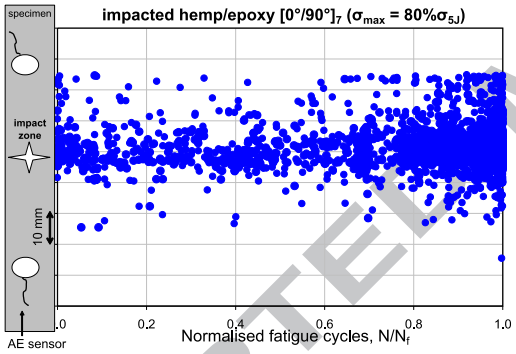


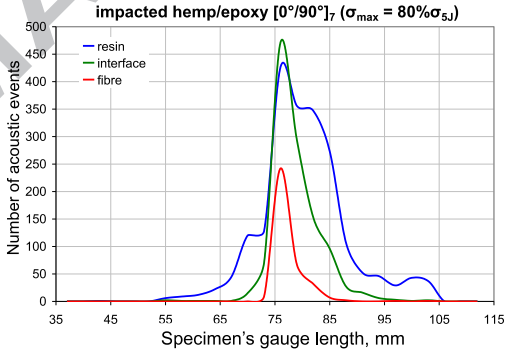

(a)

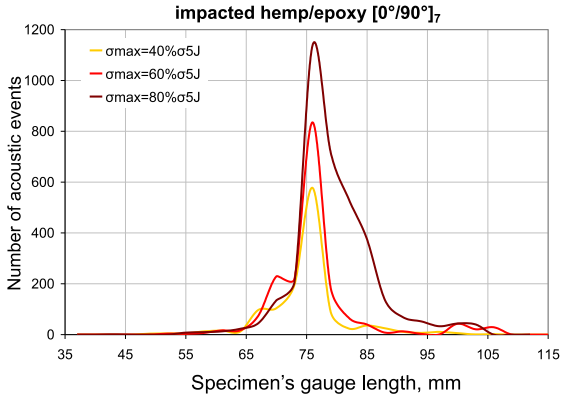


(b)

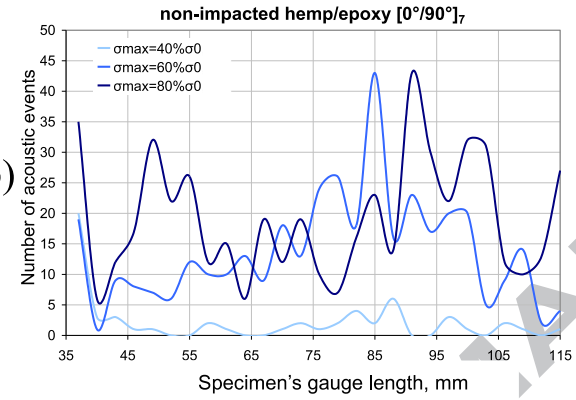

(a) impacted

(b) non impacted

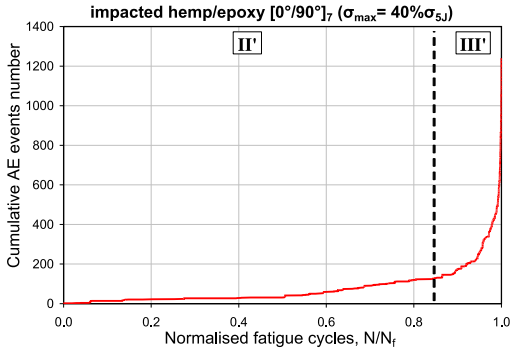


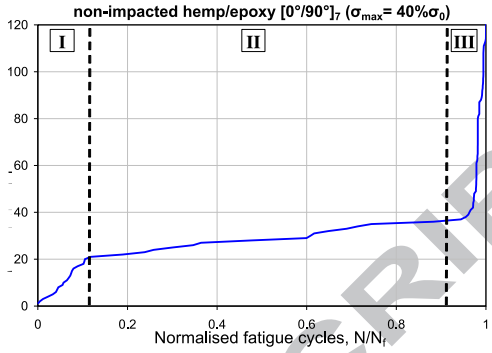


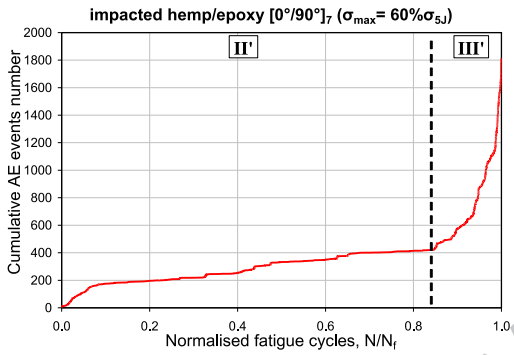


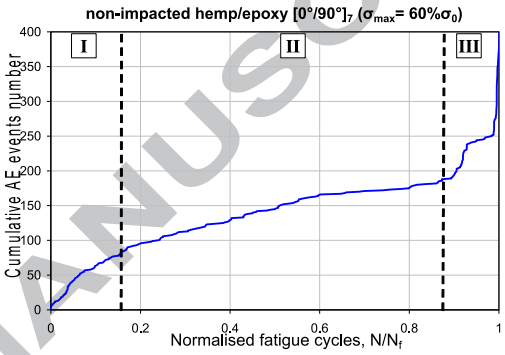


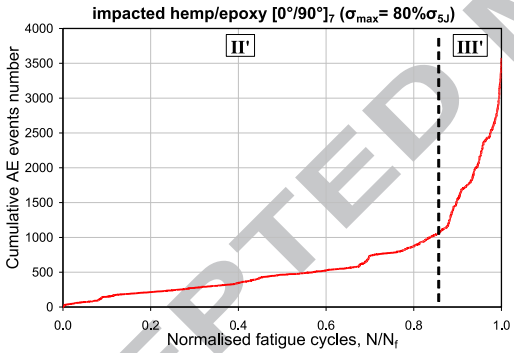


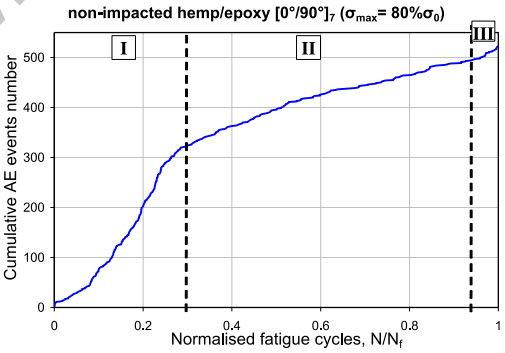

(a)

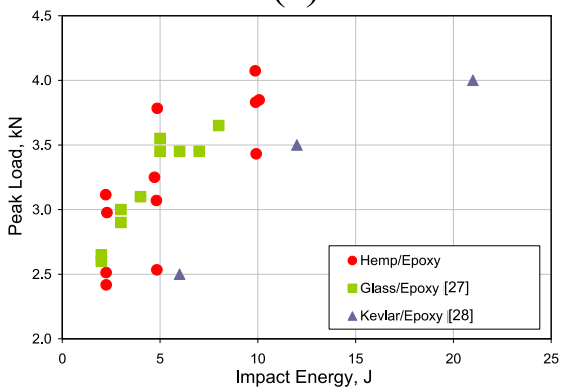


(b)

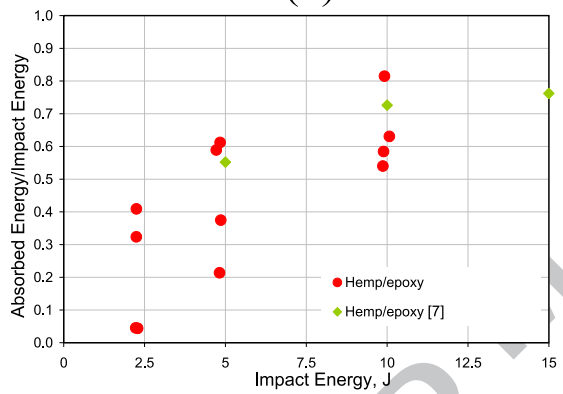

Front face

Back face

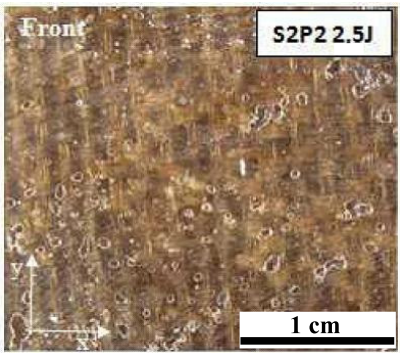


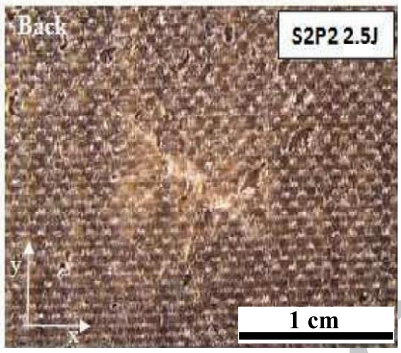


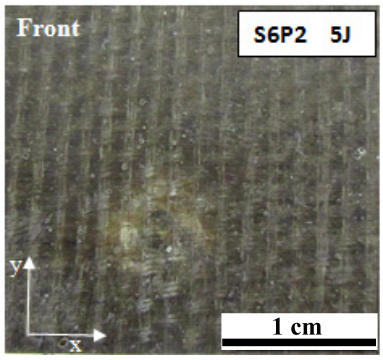


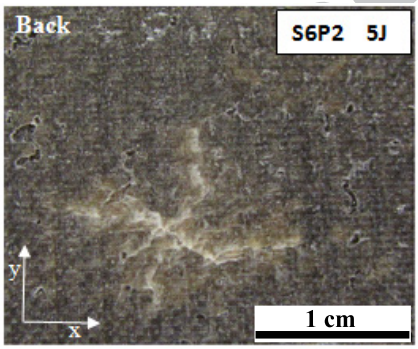


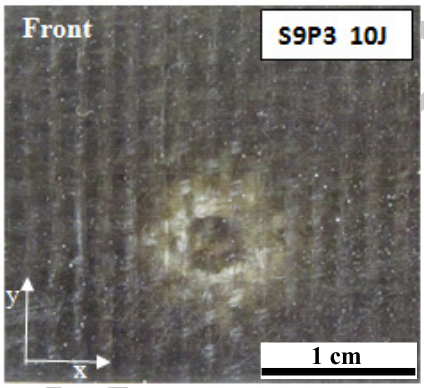


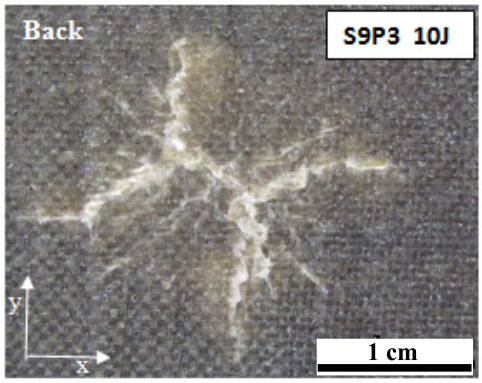

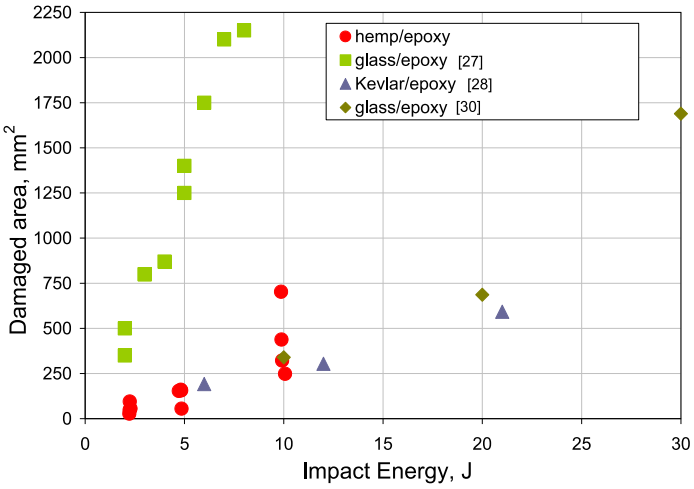
hemp/epoxy
glass/epoxy [27]
Kevlar/epoxy [28]
glass/epoxy [30]
Damaged area, mm2
Impact Energy, J
0
250
500
750
1000
1250
1500
1750
2000
2250
0
5
10
15
20
25
30

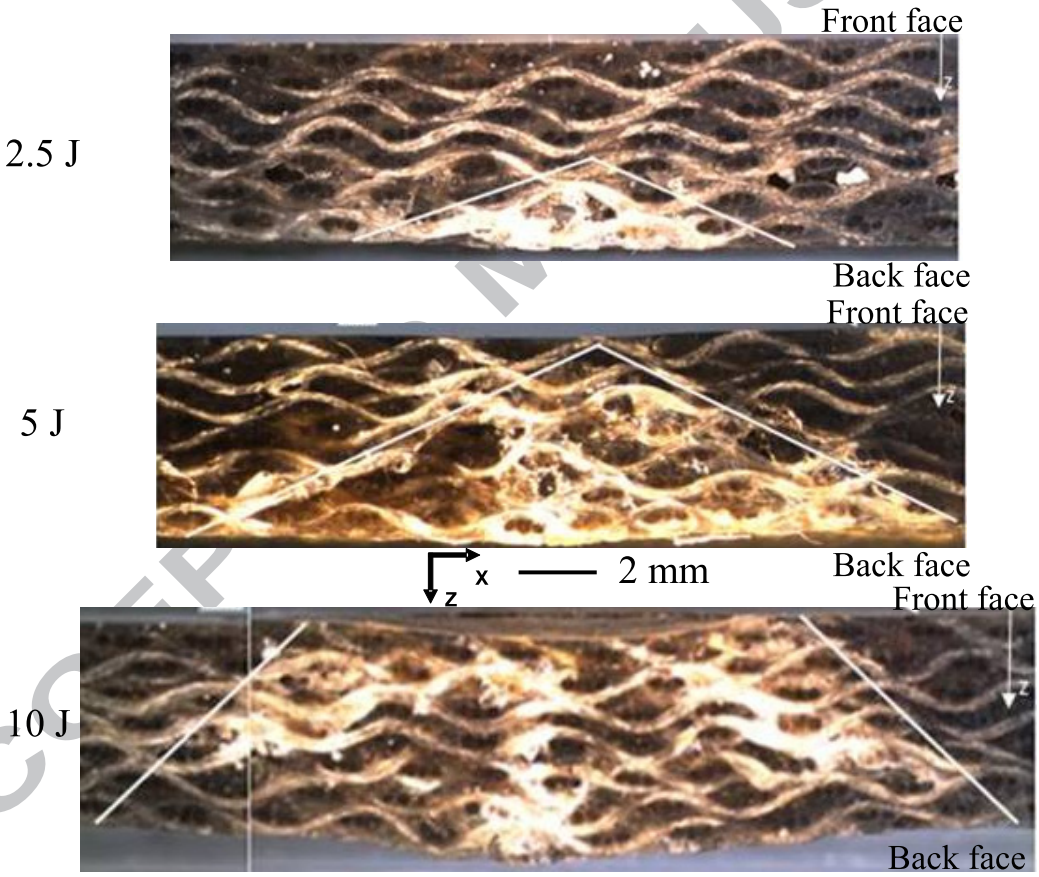
Front face
2.5 J
Back face
Front face
5 J
Back face
x
z
2 mm
Front face
10 J
Back face

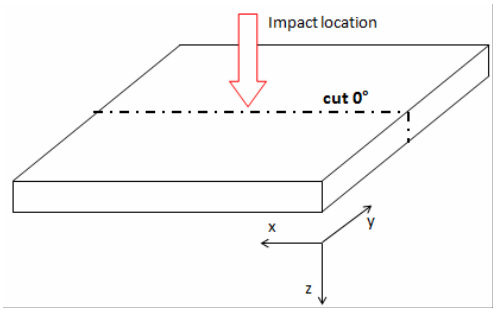


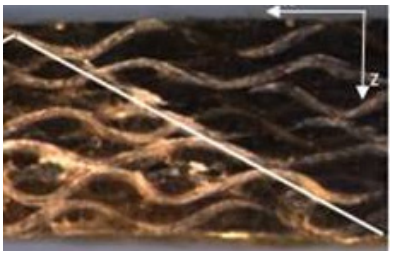


2mm

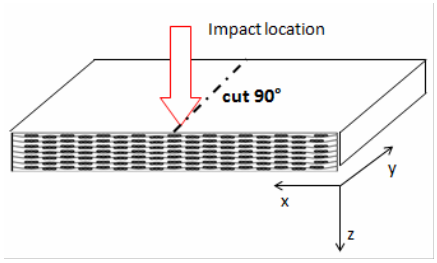


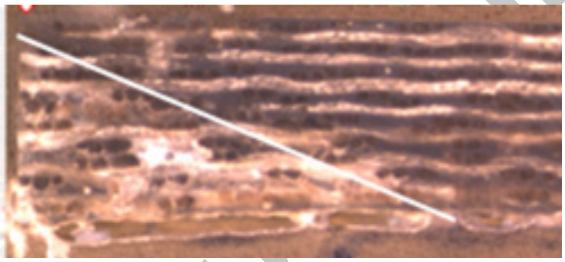

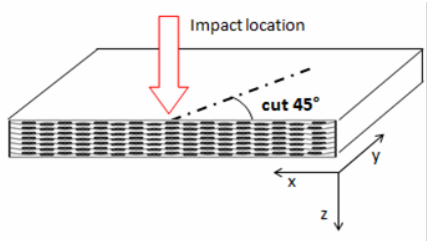


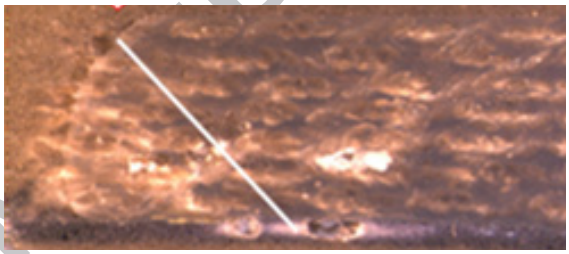

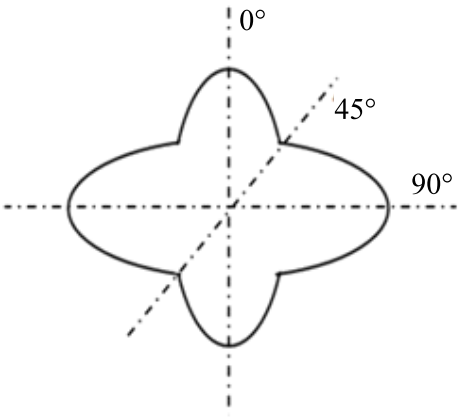

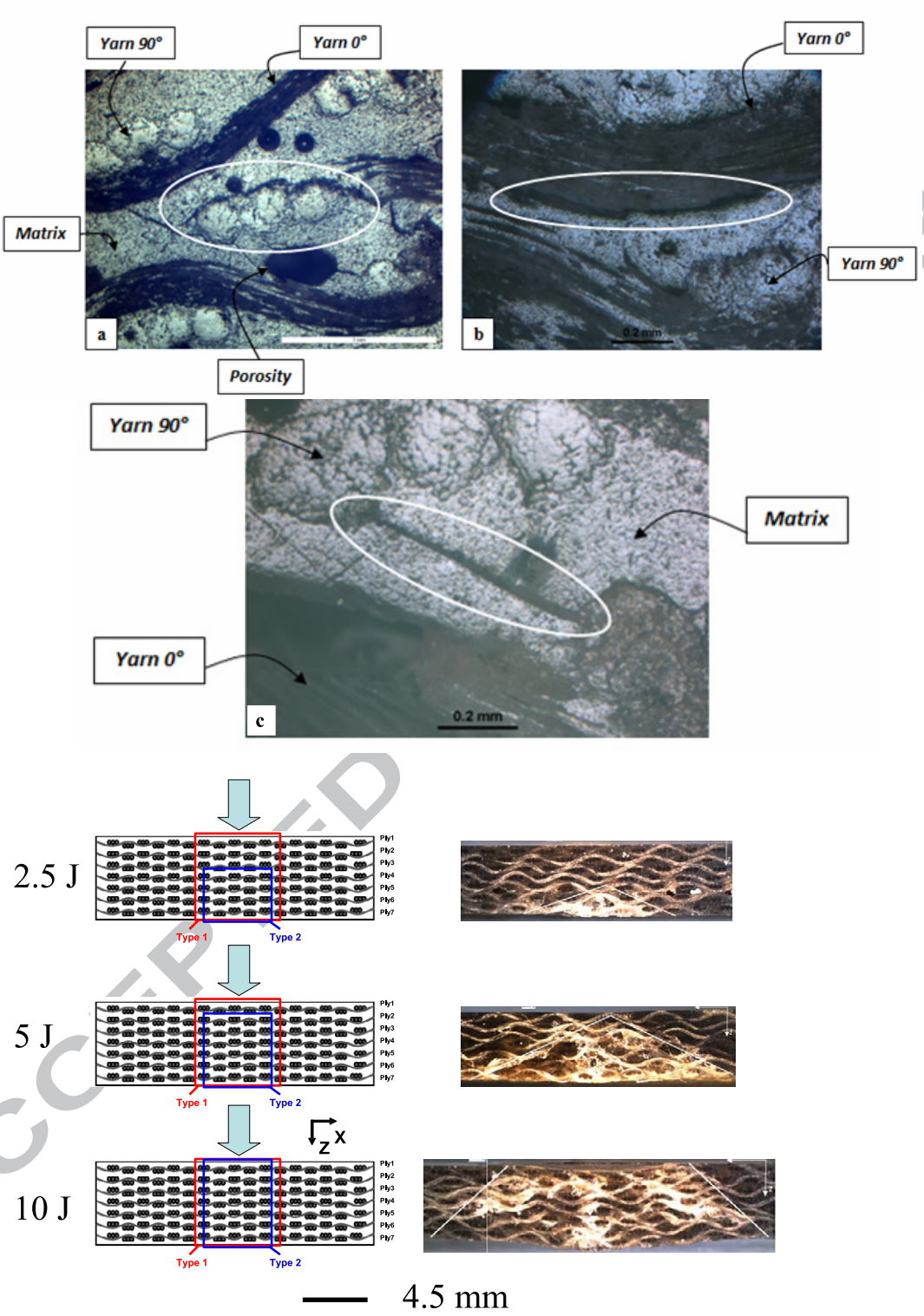
Yarn 90°
Yarn 0°
Matrix
Porosity
a
Yarn 0°
Yarn 90°
b
0.2 mm
Yarn 90°
Matrix
Yarn 0°
c
0.2 mm
2.5 J
5 J
10 J
Ply1
Ply2
Ply3
Ply4
Ply5
Ply6
Ply7
Type 1
Type 2
z
x
4.5 mm